

Scalable and Passive Wireless Network Clock Synchronization

Dave Zachariah, Satyam Dwivedi, Peter Händel and Petre Stoica

Abstract—Clock synchronization is ubiquitous in wireless systems for communication, sensing and control. In this paper we design a scalable system in which an indefinite number of passively receiving wireless units can synchronize to a single master clock at the level of discrete clock ticks. Accurate synchronization requires an estimate of the node positions. If such information is available the framework developed here takes position uncertainties into account. In the absence of such information we propose a mechanism which enables simultaneous synchronization and positioning. Furthermore we derive the Cramer-Rao bounds for the system which show that it enables synchronization accuracy at sub-nanosecond levels. Finally, we develop and evaluate an online estimation method which is statistically efficient.

I. INTRODUCTION

Time synchronization plays a key role in wireless communication, sensing and control. Indeed, many wireless applications require upkeep of timing in accomplishing their objectives.

In wireless cellular communications, accurate time information is traditionally needed for signal acquisition, demodulation, multiple access coordination, etc [1], [2]. Accurate timing and synchronization are also requirements in real-time wireless channel characterization and in several concepts in wireless communications, including beamforming and interference alignment [3]–[6]. Such requirements are also mentioned in [3] as the main challenge for distributed beamforming to work in the next generation wireless communication systems. Similarly, in [4]–[6], accurate time synchronization is shown to be a requirement for interference alignment to work. Emerging concepts like femto-cells pose more challenging synchronization requirements in terms of scalability and accuracy as discussed in [7]. The sub-nanosecond time and phase synchronization is also needed in distributed radar applications [8]. Wireless ranging and positioning require time synchronization in time-difference-of-arrival (TDOA) based schemes, where anchor nodes are synchronized in time [9]. Wireless control networks are also critically dependent on synchronized sensors and actuators [10].

Variants of the Network Time Protocol (NTP) [11] and the Precision Time Protocol (PTP) [12] constitute the most popular methods for time reference and synchronization in wired networks [13]. The emergence of a variety of wireless networks during the past decade has led to the development of wireless time-synchronization protocols and localization schemes. The Reference Broadcast Synchronization (RBS) and the Time synchronization Protocol for Sensor Networks

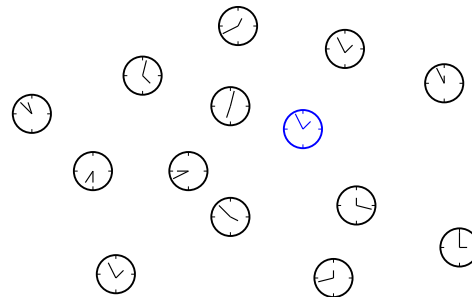


Fig. 1. Wireless network of nodes with local clocks. The highlighted clock (blue) is a transmitting master unit to which all passively receiving units should synchronize.

(TPSN) emerged as popular wireless time synchronization protocols around the same time [14], [15]. In RBS, the nodes in a wireless network synchronize through a broadcast by a master node and inter-node exchanges to remove any sender uncertainty. TPSN works by creating a hierarchical tree-based structure where every leaf node synchronizes to its parent node through message exchanges. Neither RBS nor TPSN accounts for propagation delays nor do they enable passive synchronization. For the aimed accuracies of these protocols, the signal time-of-flight over a wireless channel is assumed to be negligible. The protocol developed in [16] enables higher accuracy by using separate channels for communication and measurements required for synchronization.

Global Positioning System (GPS) signals are also used for synchronizing time in wireless communication systems [6]–[8], [17], [18]. GPS-based timing solutions enable an indefinite number of nodes to perform simultaneous self-localization and time synchronization. This joint feature is important in deployed wireless sensor networks where both position and time need to be resolved at each sensing node. In GPS-based solutions, a signal known as pulse per second (PPP) is extracted from pseudorange measurements and satellite ephemeris data at the GPS receivers. The PPP signal is then used as a reference in frequency synthesizers to generate high frequency signals [5], [8], [19]. However, GPS signals cannot be accessed indoors and the timing accuracy obtained does not reach nanosecond levels.

In this paper we develop a scalable system in which passive, receiver-only nodes can synchronize to a single master clock at the level of discrete clock ticks. We show that the synchronization performance of the system can reach sub-nanosecond levels. When position information is lacking, we propose a mechanism which enables simultaneous synchronization and

positioning at each node using three additional transceivers.

A. Prior art and our contributions

Time synchronization schemes are evolving to provide nanosecond-level synchronization, which requires accounting for signal time-of-flight between nodes. A scalable multihop scheme to synchronize the nodes to nanosecond accuracy was proposed in [20].

Several works have developed system proposals as well as presented theoretical analyses of time synchronization, cf. [21]–[23]. Fundamental limits on time synchronization in sensor networks were given in [21]. The authors of [22] suggested using factor-graph methods for network clock estimation. In [23], clock synchronization is achieved using eavesdropping measurements. The synchronizing unit is a receiver-only node and hence the method is claimed to be energy efficient. In [24] a joint localization method for source nodes was proposed using TDOA which implicitly synchronizes an arbitrary number of anchor nodes.

Our proposed method for clock synchronization in wireless networks enables system performance beyond the state-of-the-art. Specifically, we highlight the following attributes of our proposal.

- *Accuracy:* We focus on enabling nanosecond accuracy. NTP provides millisecond accuracy over IP networks and has been overtaken by PTP over wired networks. PTP provides accuracy levels of a few nanoseconds using specialized hardware. For wireless solutions, such as RBS and TPSN, the accuracy for sensor network synchronization methods is on the order of microseconds. These methods do not need to take time of flight into account as their requirements are less stringent. GPS-based synchronization methods can typically synchronize to a 100 nanosecond-level. For nanosecond levels, time of flight needs to be estimated accurately as in [20].
- *Scalability:* Another feature of the proposed synchronization method is its scalability. Scalability has been addressed previously in a few papers, albeit only implicitly. RBS, TPSN and the scheme proposed in [20] are scalable by virtue of providing synchronization to nodes through adhoc multihop connections. In these systems, nodes synchronize through mutual exchanges of signals among them. The signal exchange could be two-way round-trip time measurements or timestamps recording time-of-arrival information. By contrast, systems like GPS and the one proposed in [23] are receiver-only systems and hence they allow any number of nodes to synchronize with the reference clock. Our proposed method is similar to the latter class of scalable solutions. Indeed, we develop a method that is scalable as each synchronizing node requires only a receiver to synchronize to a reference, as in GPS. The lack of transmission requirement for the synchronizing nodes makes the solution energy efficient.
- *Positioning for synchronization:* Our proposed solution is similar to GPS with respect to scalability but enables nanosecond accuracy using existing hardware technologies. In addition, it can be used in indoor scenarios.

We will propose a local positioning system along with the synchronization mechanism to enable time-of-flight estimation. The proposed positioning system for synchronization builds upon our previous works [25]–[28].

We consider a general scenario as illustrated in Figure 1. The observed clock time in a wireless network is traditionally modeled as a continuous function of clock skew α and the phase offset β [23], [29], [30],

$$C_m(t) = t \text{ and } C_u(t) = \alpha t + \beta, \quad (1)$$

where $C_m(t)$ denotes a reference master clock and $C_u(t)$ denotes the local clock of a node u in the network. In this model the local clock time can be resolved into that of the master clock by identifying the clock parameters. Network synchronization is achieved by resolving the observed time at each node to a common clock.

In digital clocks, however, time is recorded by counting the number of periods of a repeating clock signal. At each rising clock edge of the periodic signal, an integer time counter is incremented. Our goal is to resolve the time observed on clocks at nodes $u = 1, \dots, U$. To achieve resolution levels below that of the clock period we propose using a time measuring device that can observe *intervals* between discrete time events. Such events are defined as periodic ticks on the digital clock and as received signals from the master node m .

More concretely, to enable sub-nanosecond accuracy in time synchronization, we propose the usage of:

- High bandwidth signals. As is widely documented in the literature, the precision of time of arrival measurements is inversely proportional to the square bandwidth of the transmitted signal [31], [32].
- Accurate time-interval measurement device. Examples include high speed analog-to-digital (ADC) converters and time-to-digital converters (TDC); such devices can measure time intervals with sub-nanosecond accuracy. In [20] a high speed ADC was used with sampling frequency greater than 1 Giga samples per second. In [33], clock parameter estimation for two clocks was experimentally demonstrated using a TDC with a precision of nearly 100 picoseconds.

The solution proposed in [24] is a recent, novel way of synchronizing fixed anchor nodes while estimating the positions of several emitting source nodes. In our setup, passive nodes with unknown positions can synchronize to a master node.

B. Problem formulation

The state of each digital clock is the integer number of cycles that have elapsed since some initialization event. Suppose the master clock operates with a period T_m . Then its clock state $n_m \in \{0, 1, 2, \dots\}$ corresponds to times

$$C_m \in \{0, T_m, 2T_m, \dots\}.$$

The master clock initializes the counters by transmitting a signal across the wireless network. The clock at node u , which operates with period T_u , will have a relative offset ϕ_u due to

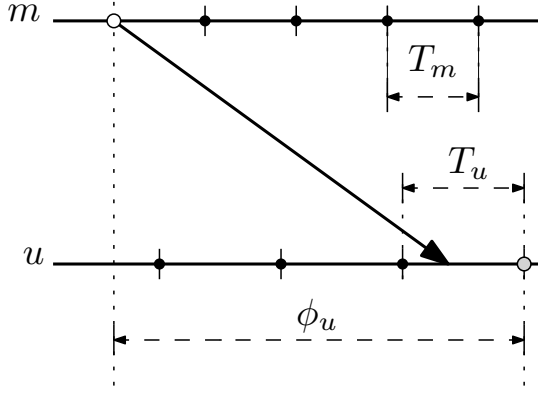


Fig. 2. Space-time diagram of nodes m and u , with one vertical spatial dimension and a horizontal time dimension. The digital clock states correspond to discrete events or ticks along the time-axes (dots). The master node m and passive node u have clock periods T_m and T_u , respectively. The transmission event from the master defines the initial tick of the system clock (white). Upon receiving the signal, the corresponding initial tick on the local clock (gray) will be subject to an unknown offset ϕ_u .

the propagation delay and nonsynchronicity as illustrated in Fig. 2. Its clock state $n_u \in \{0, 1, 2, \dots\}$ corresponds to times

$$\mathcal{C}_u \in \{\phi_u, T_u + \phi_u, 2T_u + \phi_u, \dots\}.$$

Therefore the current clock state n_u of the node can be resolved into a common time if the clock parameters ϕ_u and T_u are identified. In addition, identification of T_m enables also coordination with respect to the master periodic signal across the wireless network.

Based on the previous discussion we may write

$$\mathcal{C}_m = T_m n_m \quad \text{and} \quad \begin{cases} \mathcal{C}_1 = T_1 n_1 + \phi_1 \\ \mathcal{C}_2 = T_2 n_2 + \phi_2 \\ \vdots \\ \mathcal{C}_U = T_U n_U + \phi_U \end{cases}. \quad (2)$$

By identifying the clock parameters at each node $u = 1, \dots, U$, synchronization is achieved since a common time frame is shared across the entire network. This enables coordination relative to the master clock among all nodes.

Note that nominal values of the clock frequencies, and therefore of the periods T_u and T_m , are typically available given. However, usually, these values are not sufficiently precise. To obtain more accurate estimates of T_u it is possible to use a device that measures the intervals between ticks. Similarly, as the signal from the master clock is repeated periodically after M cycles, T_m can also be estimated accurately. The primary challenge, however, is to estimate the relative offset ϕ_u .

In this paper, we design a system in which passively receiving nodes are synchronized by estimating their respective clock parameters. The system is scalable to an indefinite number of nodes, i.e. $U \gg 1$. Furthermore, we study the resolution limits of the system using the Cramér-Rao bounds. Using existing hardware performance figures, we show that the proposed system enables sub-nanosecond accuracy. While the estimation of T_m and T_u can be performed separately from ϕ_u , we derive a joint online estimator that takes into account

the uncertainties of all estimates. The proposed estimator is subsequently evaluated in several numerical experiments.

Remark: An implementation of the estimator along with numerical simulation examples is available at the webpage of KTH Dept. Signal Processing under ‘Reproducible research’.

II. SYSTEM MODEL

To achieve the objectives stated above, we propose a system with the following features:

- 1) All passive units can measure time-intervals $\Delta = t - t'$ between events at times t and t' , using a time measurement device. This enables observations at a higher resolution than that of the digital clock and is grounded in the emerging TDC and ADC technologies.
- 2) The master periodically transmits a time-resolvable signal after M clock cycles. Among others, this ensures the identifiability of T_m . The transmission event from the master defines the starting point of a system-wide clock with period T_m . We call the period of M clock cycles an *epoch*.
- 3) The master node m is located at a known position \mathbf{x}_m . The position of an arbitrary synchronizing node u , denoted \mathbf{x} , is unknown. Together with the assumption that an epoch is longer than the clock period of any synchronizing node, i.e., $MT_m > T_u$, that fact that \mathbf{x}_m is known enables the identifiability of ϕ_u as we will show below.

We will model the unknown position as $\mathbf{x} \sim \mathcal{N}(\bar{\mathbf{x}}, \Lambda_x^{-1})$ when we have access to a prior estimate $\bar{\mathbf{x}}$ with a dispersion matrix Λ_x^{-1} . When such prior position information is lacking, i.e. when $\Lambda_x = \mathbf{0}$, then ϕ_u cannot be identified. To ensure identifiability in such a case, under the assumption that the positions are expressed in three-dimensional coordinates, we consider a system with the following additional features:

- 4) There exists three transceiving nodes, deployed at known positions $\{\mathbf{x}_1, \mathbf{x}_2, \mathbf{x}_3\}$, cf. Fig. 3. The transceivers transmit sequentially in the order $\{m, 1, 2, 3\}$, and repeatedly.
- 5) When receiving a signal from the preceding transmitter in the above order, the subsequent transceiver transmits after a fixed delay Δ_0 , which can be generated independently of the local clock [28]. This is to avoid interfering signals from the master and transceivers during an epoch. Specifically, we assume

$$MT_m \gg \Delta_0 > \max. \text{ distance to transmitter}/c,$$

where c is the propagation velocity. Then each transmitted signal can reach all nodes before the subsequent signal is transmitted.

Making use of these features together, we will show that it is possible to synchronize any number of passively receiving nodes. That is, each synchronizing node u can resolve the unknown clock parameters ϕ_u , T_u and T_m in (2). The scalable *wireless network synchronization system* is abbreviated SWINS.

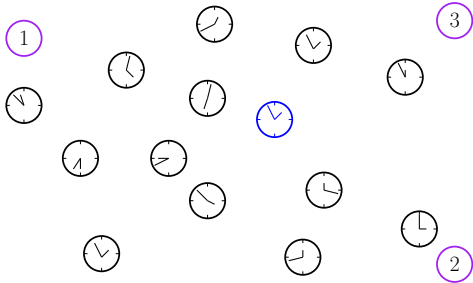


Fig. 3. System model with three additional transceivers at known positions.

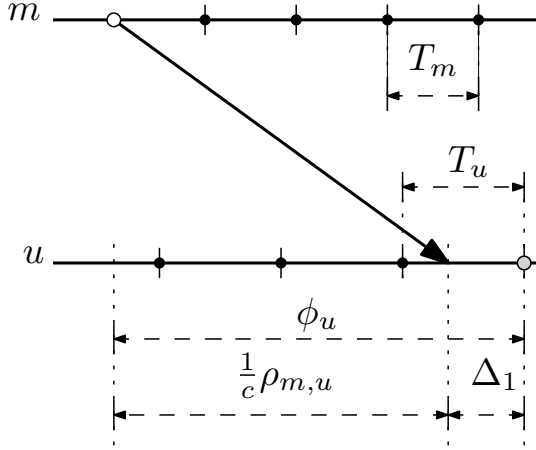


Fig. 4. Space-time diagram of nodes m and u . Δ_1 is defined as the time interval between the received signal and the subsequent clock tick at u (gray). The time of flight equals $\frac{1}{c}\rho_{m,u}$.

A. Data model

First, consider the initial signal received by a passive node u from m , as depicted in Fig. 4. Node u can only record time intervals, and we define Δ_1 as the time between the received signal and the next clock tick at u . Given that the time of flight of the signal is $\frac{1}{c}\rho_{m,u}$, where c is the signal propagation velocity and $\rho_{m,u} = \|\mathbf{x}_m - \mathbf{x}\|_2$ is the range between m and u , the following relation

$$\Delta_1 = \phi_u - \frac{1}{c}\rho_{m,u} \quad (3)$$

applies to the first epoch.

At node u , the number of clock cycles till the subsequent epoch begins, denoted N , is recorded and corresponds to a constant time interval $NT_u \geq MT_m$. Observing each N th clock tick we can derive a relation between the observed intervals as follows, see Fig. 5 which illustrates the basic principle. Let Δ_k denote the time between receiving a signal and the kN th clock tick for $k > 1$. Then it follows that $\Delta_{k-1} + NT_u = MT_m + \Delta_k$. This relation for k intervals

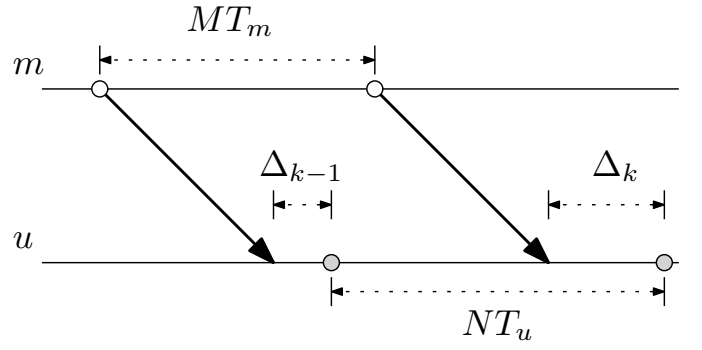


Fig. 5. Space-time diagram of nodes m and u over an epoch of M clock cycles for the master clock (white). At the local clock, each N th clock cycle is observed (gray).

together with (3) can be written as the following recursion

$$\begin{aligned} \Delta_k &= \Delta_{k-1} + NT_u - MT_m \\ &\vdots \\ \Delta_2 &= \Delta_1 + NT_u - MT_m \\ \Delta_1 &= \phi_u - \frac{1}{c}\rho_{m,u} \end{aligned}$$

which comprises the unknown clock and position parameters. Using this recursion, we can write the observed interval Δ_k at the k th epoch as

$$y_{\phi,k} = \phi_u - \frac{1}{c}\rho_{m,u} + (k-1)(NT_u - MT_m) + w_{\phi,k}, \quad (4)$$

where $w_{\phi,k}$ is a zero-mean noise. From the above equation we see that ϕ_u cannot be identified without determining also the range $\rho_{m,u}$ which is a function of the unknown position \mathbf{x} .

Next, we show that it is possible to resolve \mathbf{x} using scheduled transmissions from the three transceivers *during* an epoch. The basic principle is illustrated in Fig. 6. When the master signal reaches transceiver node 1, it transmits after a known delay Δ_0 . The subsequent transceiving nodes do the same according to the given transmission order $\{m, 1, 2, 3\}$. For the k th epoch, the time-intervals between each received signals at node u can be written as

$$\begin{aligned} y_{1,k} &= \frac{1}{c}\rho_{m,1} + \Delta_0 + \frac{1}{c}\rho_{1,u} - \frac{1}{c}\rho_{m,u} + w_{1,k}, \\ y_{2,k} &= \frac{1}{c}\rho_{1,2} + \Delta_0 + \frac{1}{c}\rho_{2,u} - \frac{1}{c}\rho_{1,u} + w_{2,k}, \\ y_{3,k} &= \frac{1}{c}\rho_{2,3} + \Delta_0 + \frac{1}{c}\rho_{3,u} - \frac{1}{c}\rho_{2,u} + w_{3,k}, \end{aligned} \quad (5)$$

where $\rho_{i,j} = \|\mathbf{x}_i - \mathbf{x}_j\|_2$. Each time-interval measurement produces a hyperbolic constraint on \mathbf{x} , cf. the principles of TDOA approach [28]. Thus three constraints are sufficient for identifying \mathbf{x} in the three-dimensional space, and therefore also for resolving ϕ_u .

At the end of the k th epoch, its duration is recorded, resulting in

$$y_{m,k} = MT_m + w_{m,k}, \quad (6)$$

where M is known and therefore we can resolve T_m from (5). Similarly, for each epoch at u , N ticks are recorded at the

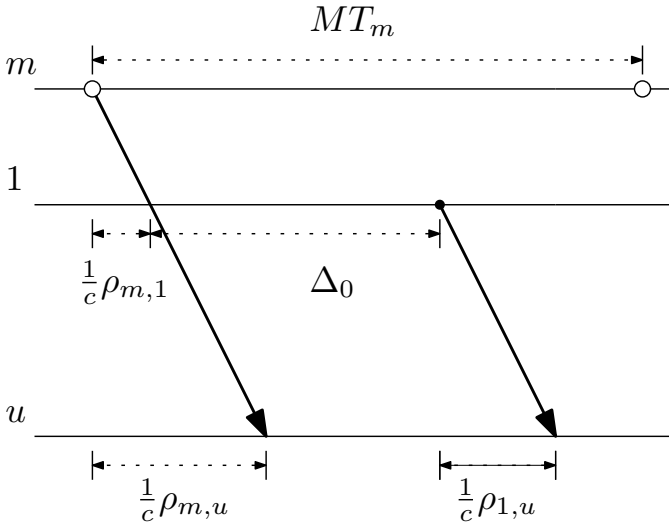


Fig. 6. Space-time diagram of nodes m , 1 and u over an epoch. Upon receiving a signal, the transceiving node 1 transmits its signal after a known delay Δ_0 . The interval between the received signals at u is: $\frac{1}{c}\rho_{m,1} + \Delta_0 + \frac{1}{c}\rho_{1,u} - \frac{1}{c}\rho_{m,u}$. Note that the apparent congruence with Δ_0 is a coincidence of the example in one-dimensional space and does not hold in general.

local clock, and the observed time interval is

$$y_{u,k} = NT_u + w_{u,k}. \quad (7)$$

In sum, using the above observations, made at a passive node u , ensures that ϕ_u , T_u and T_m are identifiable parameters. This enables wireless synchronization to the master clock m . The additional transceivers also render \mathbf{x} identifiable and therefore enable self-localization at each node u .

B. Noise model

Each observed time-interval above is subject to two sources of error arising from its start and stop events, respectively. In (5) and (6), the start and stop events are triggered by uncorrelated RF signals. A nominal value of error variance σ_0^2 from such events can be assigned but in practice varying RF conditions produce outliers so that we assume a varying σ_k^2 . The total noise variance for these measured intervals is $E[w_{i,k}^2] = 2\sigma_k^2$ for $i = m, 1, 2, 3$ since they are based on a pair of RF measurements. In (6), one RF measurement is shared with (4) so that the errors of the observed intervals are correlated: $E[w_{\phi,k}w_{m,k}] = \sigma_k^2$. Furthermore, because two consecutive measurements share one RF measurement in (6) and (5), we can write:

$$E[w_{i,k}w_{j,k}] = \begin{cases} 2\sigma_k^2, & i = j \\ \sigma_k^2, & j \text{ follows } i, \text{ or vice versa,} \\ 0, & \text{otherwise.} \end{cases}$$

We assume that the RF noise yields the dominant part of σ_k and that the noise contribution of the timing device itself is only a small fraction $0 < \alpha < 1$ of σ_k , which depends on the performance figures of the device. In practice $\alpha = 0.1$ is a reasonable value for existing hardware [33], and this is the value we will assume in what follows. Then since the start

and stop events of the interval in (7) are triggered solely by two clock ticks, we have $E[w_{u,k}^2] = 2\alpha^2\sigma_k^2$. Finally, because (4) is based on one RF and one clock tick we have $E[w_{\phi,k}^2] = (1 + \alpha^2)\sigma_k^2$. We model the noise sources as jointly Gaussian and omit the correlation between consecutive epochs.

III. CRAMÉR-RAO BOUNDS

To study some basic properties of SWINS, we begin by collecting the observed time intervals from epoch k in a vector

$$\mathbf{y}_k \triangleq \mathbf{S}_k [y_{\phi,k} \ y_{u,k} \ y_{m,k} \ y_{1,k} \ y_{2,k} \ y_{3,k}]^\top \in \mathbb{R}^{n_k}, \quad (8)$$

where

$$\mathbf{S}_k = \begin{cases} \mathbf{I}_6 & \text{if transceiving nodes present in epoch } k, \\ [\mathbf{I}_3 \ \mathbf{0}_{3 \times 3}] & \text{otherwise} \end{cases} \quad (9)$$

is a selection matrix and n_k is the number of measured intervals in epoch k . Combining (4), (7), (6), and (5), we can write (8) as

$$\mathbf{y}_k = \boldsymbol{\mu}_k + \mathbf{H}_k \mathbf{c} + \frac{1}{c} \mathbf{G}_k \boldsymbol{\rho}(\mathbf{x}) + \mathbf{w}_k \in \mathbb{R}^{n_k}, \quad (10)$$

where $\mathbf{c} \triangleq [\phi_u \ T_u \ T_m]^\top$ contains the parameters of interest. The mean vector

$$\boldsymbol{\mu}_k = \mathbf{S}_k \begin{bmatrix} 0 \\ 0 \\ 0 \\ \frac{1}{c} \|\mathbf{x}_m - \mathbf{x}_1\| + \Delta_0 \\ \frac{1}{c} \|\mathbf{x}_1 - \mathbf{x}_2\| + \Delta_0 \\ \frac{1}{c} \|\mathbf{x}_2 - \mathbf{x}_3\| + \Delta_0 \end{bmatrix} \in \mathbb{R}^{n_k}$$

is known and the vector of ranges

$$\boldsymbol{\rho}(\mathbf{x}) = \begin{bmatrix} \|\mathbf{x} - \mathbf{x}_m\|_2 \\ \|\mathbf{x} - \mathbf{x}_1\|_2 \\ \|\mathbf{x} - \mathbf{x}_2\|_2 \\ \|\mathbf{x} - \mathbf{x}_3\|_2 \end{bmatrix} \in \mathbb{R}^4,$$

is a function of the unknown position \mathbf{x} . The known system matrices in (10) can be written as

$$\mathbf{H}_k = \mathbf{S}_k \begin{bmatrix} 1 & (k-1)N & -(k-1)M \\ 0 & N & 0 \\ 0 & 0 & M \\ 0 & 0 & 0 \\ 0 & 0 & 0 \\ 0 & 0 & 0 \end{bmatrix},$$

$$\mathbf{G}_k = \mathbf{S}_k \begin{bmatrix} -1 & 0 & 0 & 0 \\ 0 & 0 & 0 & 0 \\ 0 & 0 & 0 & 0 \\ -1 & 1 & 0 & 0 \\ 0 & -1 & 1 & 0 \\ 0 & 0 & -1 & 1 \end{bmatrix}.$$

Based on the noise model introduced in Section II-B, the measurement noise vector \mathbf{w}_k has a covariance matrix

$\sigma_k^2 \mathbf{Q}_k \triangleq \mathbb{E}[\mathbf{w}_k \mathbf{w}_k^\top]$, given by:

$$\mathbf{Q}_k = \mathbf{S}_k \begin{bmatrix} (1 + \alpha^2) & 0 & 1 & 0 & 0 & 0 \\ 0 & 2\alpha^2 & 0 & 0 & 0 & 0 \\ 1 & 0 & 2 & 1 & 0 & 0 \\ 0 & 0 & 1 & 2 & 1 & 0 \\ 0 & 0 & 0 & 1 & 2 & 1 \\ 0 & 0 & 0 & 0 & 1 & 2 \end{bmatrix} \mathbf{S}_k^\top.$$

As the noise \mathbf{w}_k is modeled as Gaussian, we have

$$\mathbf{y}_k | \mathbf{c}, \mathbf{x}, \sigma_k^2 \sim \mathcal{N}(\boldsymbol{\mu}_k + \mathbf{H}_k \mathbf{c} + \frac{1}{c} \mathbf{G}_k \boldsymbol{\rho}(\mathbf{x}), \sigma_k^2 \mathbf{Q}_k). \quad (11)$$

This data model enables an analysis of how accurately the clock parameters can be estimated in SWINS.

A. Cramér-Rao bound

Define the vector

$$\boldsymbol{\theta} \triangleq \begin{bmatrix} \mathbf{c} \\ \mathbf{x} \end{bmatrix} \in \mathbb{R}^{3+d},$$

where $d = 2$ or 3 is the spatial dimension. The Fisher information matrix of $\boldsymbol{\theta}$ for the k th epoch data model in (11) is given by [34, ch. 3] [35, App. B.3]:

$$\mathbf{J}_k(\mathbf{x}, \sigma_k^2) = \frac{1}{\sigma_k^2} \left[\mathbf{H}_k \quad \frac{1}{c} \mathbf{G}_k \boldsymbol{\Gamma}(\mathbf{x}) \right]^\top \mathbf{Q}_k^{-1} \left[\mathbf{H}_k \quad \frac{1}{c} \mathbf{G}_k \boldsymbol{\Gamma}(\mathbf{x}) \right], \quad (12)$$

where the Jacobian of the range function $\boldsymbol{\rho}(\mathbf{x})$ is

$$\boldsymbol{\Gamma}(\mathbf{x}) \triangleq \partial_{\mathbf{x}} \boldsymbol{\rho}(\mathbf{x}) = \begin{bmatrix} \frac{(\mathbf{x} - \mathbf{x}_m)^\top}{\|\mathbf{x} - \mathbf{x}_m\|_2} \\ \frac{(\mathbf{x} - \mathbf{x}_1)^\top}{\|\mathbf{x} - \mathbf{x}_1\|_2} \\ \frac{(\mathbf{x} - \mathbf{x}_2)^\top}{\|\mathbf{x} - \mathbf{x}_2\|_2} \\ \frac{(\mathbf{x} - \mathbf{x}_3)^\top}{\|\mathbf{x} - \mathbf{x}_3\|_2} \end{bmatrix} \in \mathbb{R}^{4 \times d}.$$

In the above model, the data from each epoch are mutually uncorrelated. Therefore the information from each epoch is additive and the total information matrix after k epochs equals

$$\boldsymbol{\Lambda}_k = \boldsymbol{\Lambda}_{k-1} + \mathbf{J}_k, \quad (13)$$

where $\boldsymbol{\Lambda}_0 = \mathbf{0}$. Then the mean-square error (MSE) matrix of any unbiased estimator $\hat{\boldsymbol{\theta}}$ is bounded via the Cramér-Rao inequality:

$$\mathbb{E}_y[(\boldsymbol{\theta} - \hat{\boldsymbol{\theta}})(\boldsymbol{\theta} - \hat{\boldsymbol{\theta}})^\top] \succeq \boldsymbol{\Lambda}_k^{-1},$$

and specifically for $\hat{\mathbf{c}}$ we have

$$\mathbb{E}_y[(\mathbf{c} - \hat{\mathbf{c}})(\mathbf{c} - \hat{\mathbf{c}})^\top] \succeq (\boldsymbol{\Lambda}_{c,k} - \boldsymbol{\Lambda}_{xc,k}^\top \boldsymbol{\Lambda}_{x,k}^{-1} \boldsymbol{\Lambda}_{xc,k})^{-1}, \quad (14)$$

where the right-hand side is obtained by partitioning the information matrix as

$$\boldsymbol{\Lambda}_k = \begin{bmatrix} \boldsymbol{\Lambda}_{c,k} & \boldsymbol{\Lambda}_{xc,k}^\top \\ \boldsymbol{\Lambda}_{xc,k} & \boldsymbol{\Lambda}_{x,k} \end{bmatrix}.$$

Note that the information matrix, via (12), is dependent on \mathbf{x} and σ_k^2 , but not on the clock parameters \mathbf{c} .

To illustrate the spatial dependence of $\boldsymbol{\Lambda}_k$ on \mathbf{x} , for $d = 2$, we plot the Cramér-Rao bound (CRB) of ϕ_u as a function of

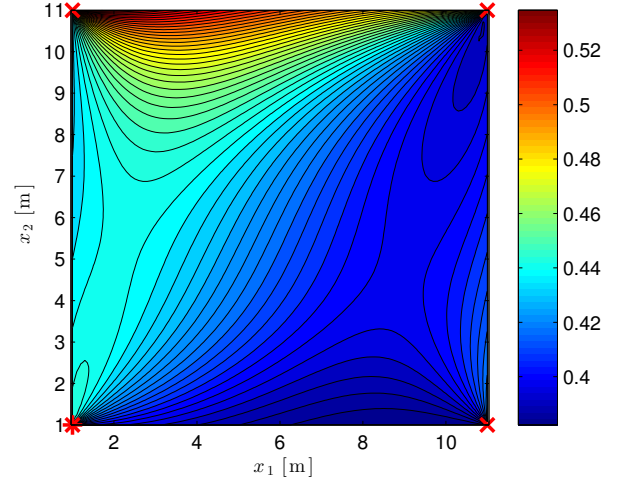


Fig. 7. Resolution limit of ϕ_u in [ns], using the square-root of the CRB, as a function of \mathbf{x} . The noise level σ_k is fixed to 5 [ns] and 250 epochs are observed. The master and transceiver locations are denoted by an asterisk and by crosses, respectively.

\mathbf{x} in Fig. 7. We set the known positions of the master and transceivers as

$$\mathbf{x}_m = \begin{bmatrix} 1 \\ 1 \end{bmatrix}, \mathbf{x}_1 = \begin{bmatrix} 11 \\ 11 \end{bmatrix}, \mathbf{x}_2 = \begin{bmatrix} 1 \\ 11 \end{bmatrix}, \mathbf{x}_3 = \begin{bmatrix} 11 \\ 1 \end{bmatrix}. \quad (15)$$

The noise standard deviation σ_k is fixed to 5 [ns] and the fraction arising from the timing device is set to $\alpha = 0.1$, which are reasonable figures for existing hardware technologies. Using 250 epochs we see that the resolution limit of SWINS is on the order of sub-nanoseconds across space. We note in the passing that the spatial configuration of the transmitting nodes $\{m, 1, 2, 3\}$ and their transmission order result in a slightly lower limit in the bottom right quadrant.

B. Hybrid Cramér-Rao bound

When an informative prior for \mathbf{x} exists, the unknown position can be modeled as a random variable $\mathbf{x} \sim \mathcal{N}(\bar{\mathbf{x}}, \boldsymbol{\Lambda}_x^{-1})$. Then the MSE matrix of any unbiased estimator $\hat{\mathbf{c}}$, when averaged over all possible values of \mathbf{x} , is bounded via the Hybrid Cramér-Rao inequality [36]:

$$\mathbb{E}_{y,x}[(\mathbf{c} - \hat{\mathbf{c}})(\mathbf{c} - \hat{\mathbf{c}})^\top] \succeq (\bar{\boldsymbol{\Lambda}}_{c,k} - \bar{\boldsymbol{\Lambda}}_{xc,k}^\top \bar{\boldsymbol{\Lambda}}_{x,k}^{-1} \bar{\boldsymbol{\Lambda}}_{xc,k})^{-1}, \quad (16)$$

where the right-hand side is obtained from the expected information matrix

$$\bar{\boldsymbol{\Lambda}}_k = \mathbb{E}_x[\boldsymbol{\Lambda}_k] + \begin{bmatrix} \mathbf{0} & \mathbf{0} \\ \mathbf{0} & \boldsymbol{\Lambda}_x \end{bmatrix} = \begin{bmatrix} \bar{\boldsymbol{\Lambda}}_{c,k} & \bar{\boldsymbol{\Lambda}}_{xc,k}^\top \\ \bar{\boldsymbol{\Lambda}}_{xc,k} & \bar{\boldsymbol{\Lambda}}_{x,k} \end{bmatrix}.$$

The expectation is approximated numerically using Monte Carlo simulations.

To illustrate the spatial variation of (16) for $d = 2$, we drop the transceiving nodes and plot in Fig. 8 the Hybrid Cramér-Rao Bound (HCRB) of ϕ_u as a function of the prior mean $\bar{\mathbf{x}}$. The master position and the precision matrix of the prior of \mathbf{x} are given by:

$$\mathbf{x}_m = \begin{bmatrix} 1 \\ 1 \end{bmatrix}, \quad \boldsymbol{\Lambda}_x = \begin{bmatrix} 0.1^2 & 0 \\ 0 & 0.01^2 \end{bmatrix}^{-1}.$$

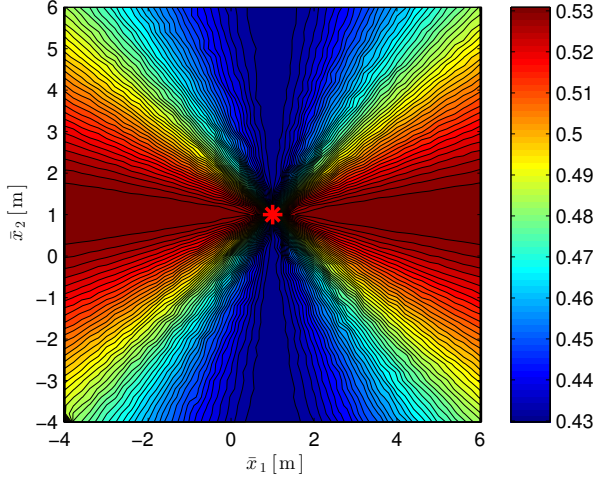


Fig. 8. Resolution limit of ϕ_u in [ns], using the square-root of the HCRB, as a function of the prior mean $\bar{\mathbf{x}}$. The noise level σ_k is fixed to 5 [ns] and 250 epochs are observed. The master location \mathbf{x}_m is denoted by an asterisk.

This corresponds to an position error ellipse whose axis correspond to standard deviations of 0.1 and 0.01 meters, respectively. There is greater uncertainty along the \bar{x}_2 -axis than the \bar{x}_1 -axis. Consequently the bound on the clock error, which depends on the range to the master, is greater when $\bar{\mathbf{x}}$ is on positions along one axis than the other. This variation in the resolution limit is clearly visible in Fig. 8. Observe that the prior precision of \mathbf{x} is sufficient to enable sub-nanosecond accuracy.

IV. ONLINE ESTIMATOR

In this section, we derive an online estimator for the clock parameters \mathbf{c} and position \mathbf{x} . The method refines the estimate at each epoch k . Its overall memory requirement is constant and computational complexity scales linearly with k .

A. Linear combiner

Our interest here is to process the data from each epoch \mathbf{y}_k sequentially and then form a linear combination of the so-obtained estimates. This combined estimate is recursively computed and, as we will see, attains the Cramér-Rao bounds of the system asymptotically.

The prior knowledge about the position can be equivalently expressed as $\bar{\mathbf{x}} \sim \mathcal{N}(\bar{\mathbf{x}}, \Lambda_x^{-1})$. Then for epoch k , we can formulate the maximum likelihood estimate

$$\check{\boldsymbol{\theta}}_k = \arg \max_{\boldsymbol{\theta}} \left[\max_{\sigma_k^2} p(\mathbf{y}_k, \bar{\mathbf{x}} | \boldsymbol{\theta}, \sigma_k^2) \right], \quad (17)$$

where $p(\mathbf{y}_k, \bar{\mathbf{x}} | \boldsymbol{\theta}, \sigma_k^2) = p(\mathbf{y}_k | \boldsymbol{\theta}, \sigma_k^2) p(\bar{\mathbf{x}} | \mathbf{x})$.

The data obtained up to epoch k produce via (17) a sequence of estimates $\check{\boldsymbol{\theta}}_1, \check{\boldsymbol{\theta}}_2, \dots, \check{\boldsymbol{\theta}}_k$. The MSE-optimal combination of the estimates is formed using weights based on the inverse covariance matrix for each estimate [37]. For epoch k , the latter is well approximated by the Fisher information matrix in

(12), or by an estimate of it which we denote $\hat{\mathbf{J}}_k$. For notational simplicity let

$$\check{\boldsymbol{\theta}}_0 = \begin{bmatrix} \mathbf{0} \\ \bar{\mathbf{x}} \end{bmatrix} \quad \text{and} \quad \hat{\mathbf{J}}_0 = \begin{bmatrix} \mathbf{0} & \mathbf{0} \\ \mathbf{0} & \Lambda_x \end{bmatrix} \quad (18)$$

denote the prior estimate and the corresponding information matrix, respectively. Then we can compute the following linear combination recursively:

$$\hat{\boldsymbol{\theta}}_k = \left(\sum_{i=0}^k \hat{\mathbf{J}}_i \right)^{-1} \left(\sum_{i=0}^k \hat{\mathbf{J}}_i \check{\boldsymbol{\theta}}_i \right) = \hat{\Lambda}_k^{-1} \mathbf{s}_k \quad (19)$$

where

$$\begin{cases} \hat{\Lambda}_k &= \hat{\Lambda}_{k-1} + \hat{\mathbf{J}}_k \\ \mathbf{s}_k &= \mathbf{s}_{k-1} + \hat{\mathbf{J}}_k \check{\boldsymbol{\theta}}_k \end{cases} \quad \text{and} \quad \begin{cases} \hat{\Lambda}_0 &= \hat{\mathbf{J}}_0 \\ \mathbf{s}_0 &= \hat{\mathbf{J}}_0 \check{\boldsymbol{\theta}}_0. \end{cases}$$

Remark: If a constant noise level σ_0^2 is used in (12), i.e., $\hat{\mathbf{J}}_k = \mathbf{J}_k(\bar{\mathbf{x}}_k, \sigma_0^2)$, then one can verify that (19) is invariant to the nominal value $\sigma_0^2 > 0$. To make (19) robust with respect to noise outliers the corresponding estimate of $\mathbf{J}_k \succ \mathbf{0}$ should decrease when there are outlying observations in epoch k . This can be achieved using the estimated noise variance from (17) for each epoch, which we denote $\check{\sigma}_k^2$. More concretely, we use $\hat{\sigma}_k^2 = \max(\check{\sigma}_k^2, \sigma_0^2)$. In this way, the estimator adapts to noise outliers that exceed a nominal σ_0^2 and at the same time occasional overestimation of the information matrix is prevented when $\check{\sigma}_k^2$ is small.

B. Minimization method

We propose a computationally efficient gradient-based method to solve (17). First we note that the negative log-likelihood can be expressed as

$$-\ln p(\mathbf{y}_k, \bar{\mathbf{x}} | \boldsymbol{\theta}, \sigma_k^2) = \frac{\sigma_k^{-2}}{2} \|\mathbf{y}_k - \boldsymbol{\mu}_k - \mathbf{H}_k \mathbf{c} - \frac{1}{c} \mathbf{G}_k \boldsymbol{\rho}(\mathbf{x})\|_{\mathbf{Q}_k}^2 + \frac{n_k}{2} \ln \sigma_k^2 + \frac{1}{2} \|\mathbf{x} - \bar{\mathbf{x}}\|_{\Lambda_x}^2 + K, \quad (20)$$

where K is a constant. We will subsequently drop the subindex k for notational convenience. The minimizing \mathbf{c} and σ^2 can be expressed as

$$\begin{aligned} \check{\mathbf{c}}(\mathbf{x}) &= (\mathbf{H}^\top \mathbf{Q}^{-1} \mathbf{H})^\dagger \mathbf{H}^\top \mathbf{Q}^{-1} (\mathbf{y} - \boldsymbol{\mu} - c^{-1} \mathbf{G} \boldsymbol{\rho}(\mathbf{x})) \\ \check{\sigma}^2(\mathbf{x}) &= \frac{1}{n} \left\| \Pi_{\mathbf{H}}^\perp (\mathbf{y} - \boldsymbol{\mu} - c^{-1} \mathbf{G} \boldsymbol{\rho}(\mathbf{x})) \right\|_{\mathbf{Q}^{-1}}^2 \end{aligned} \quad (21)$$

where

$$\Pi_{\mathbf{H}}^\perp \triangleq \mathbf{I} - \mathbf{H}(\mathbf{H}^\top \mathbf{Q}^{-1} \mathbf{H})^\dagger \mathbf{H}^\top \mathbf{Q}^{-1}$$

is a projector matrix. After inserting (21) into (20), the maximum likelihood estimate of \mathbf{x} can be obtained by solving

$$\check{\mathbf{x}} = \arg \min_{\mathbf{x}} \underbrace{\ln V_0(\mathbf{x}) + V_1(\mathbf{x})}_{\triangleq V(\mathbf{x})}, \quad (22)$$

where

$$V_0(\mathbf{x}) = \check{\sigma}^2(\mathbf{x}) \quad \text{and} \quad V_1(\mathbf{x}) = \frac{1}{n} \|\mathbf{x} - \bar{\mathbf{x}}\|_{\Lambda_x}^2. \quad (23)$$

The gradient of $V(\mathbf{x})$ can be written as

$$\partial V(\mathbf{x}) = \frac{1}{V_0(\mathbf{x})} \partial V_0(\mathbf{x}) + \partial V_1(\mathbf{x}),$$

where compact expressions of the gradients $\partial V_0(\mathbf{x})$ and $\partial V_1(\mathbf{x})$ are given in Appendix A. Starting from an initial point $\check{\mathbf{x}}^0$, we formulate a gradient descent method

$$\check{\mathbf{x}}^{i+1} = \check{\mathbf{x}}^i + \alpha_i \mathbf{p}_i, \quad (24)$$

where

$$\mathbf{p}_i \triangleq -\frac{\partial V_0(\mathbf{x}) + V_0(\mathbf{x}) \partial V_1(\mathbf{x})}{\|\partial V_0(\mathbf{x}) + V_0(\mathbf{x}) \partial V_1(\mathbf{x})\|} \propto -\partial V(\mathbf{x}) \quad (25)$$

and the step size α_i is chosen by a line search

$$\min_{\alpha_i \in I} V(\check{\mathbf{x}}^i + \alpha_i \mathbf{p}_i) \quad (26)$$

in the interval $I = [0, \eta \|\check{\mathbf{x}}^i - \check{\mathbf{x}}^{i-1}\|]$ where η is a user parameter which determines the upper limit on the step size. When prior information is available the initial point can be taken as $\check{\mathbf{x}}^0 = \bar{\mathbf{x}}$. If it is unavailable the centroid of the known transmitting node coordinates, i.e. $\check{\mathbf{x}}^0 = \frac{1}{4} \sum_i \mathbf{x}_i$, or the estimate from a previous epoch can be used.

In summary, for each epoch, (17) is solved by iterating (24) until convergence, followed by insertion of the position estimate into (21). Then a optimal estimate of θ is formed via (19). A summarizing pseudo-code is given in Algorithm 1.

Algorithm 1 Online estimator at a generic epoch

- 1: Input: \mathbf{y} , \mathbf{s} and $\hat{\Lambda}$
 - 2: Initialize $i = 0$ and $\check{\mathbf{x}}^i$
 - 3: **repeat**
 - 4: Compute \mathbf{p}_i via (25)
 - 5: Set α_i using (26)
 - 6: $\check{\mathbf{x}}^{i+1} = \check{\mathbf{x}}^i + \alpha_i \mathbf{p}_i$
 - 7: $i := i + 1$
 - 8: **until** $\alpha_i < \epsilon$
 - 9: Compute $\check{\mathbf{c}}$ and $\check{\sigma}$ via (21)
 - 10: Compute $\hat{\mathbf{J}}$ via (12)
 - 11: $\Lambda := \Lambda + \hat{\mathbf{J}}$
 - 12: $\mathbf{s} := \mathbf{s} + \hat{\mathbf{J}} \theta$
 - 13: $\hat{\theta} = \hat{\Lambda}^{-1} \mathbf{s}$
 - 14: Output: $\hat{\theta}$, \mathbf{s} and $\hat{\Lambda}$
-

V. NUMERICAL EXPERIMENTS

We perform a numerical evaluation of SWINS, comparing the accuracy of the online estimator with the Cramér-Rao bounds. The root mean-square error (RMSE) of the parameter estimates was computed using 10^3 Monte Carlo simulations.

In the following examples we set the unknown clock parameters to $T_m = 50 \times 10^{-9}$ and $T_u = 50 \times 10^{-9}$ [s]. The unknown ϕ_u contains the time of flight and the offset Δ_1 that we set to 5×10^{-9} [s]. Note however that the bounds are invariant to these parameter values. The numbers of clock

cycles were set to $M = 100$ and to $N = 101$. In all examples the master is located at the following coordinates

$$\mathbf{x}_m = \begin{bmatrix} 1 \\ 1 \end{bmatrix}.$$

In the first scenario we consider a situation in which we have prior information about the position, modeled by the distribution $\mathcal{N}(\bar{\mathbf{x}}, \Lambda_x^{-1})$, and no additional transceivers are present. In the second scenario, we consider no prior information (i.e. $\Lambda_x = \mathbf{0}$) but add transceivers located at

$$\mathbf{x}_1 = \begin{bmatrix} 11 \\ 11 \end{bmatrix}, \mathbf{x}_2 = \begin{bmatrix} 1 \\ 11 \end{bmatrix} \text{ and } \mathbf{x}_3 = \begin{bmatrix} 11 \\ 1 \end{bmatrix},$$

cf. the configuration in Fig. 7.

For the online estimator we set the nominal σ_0 to 10 [ns] and let the estimator adapt to noise outliers that exceed σ_0^2 . The upper limit on the relative step size, η , is set to 1.2. We set the tolerance ϵ to 10^{-7} .

A. Master node and no transceivers

In the first scenario, the prior information is given by

$$\bar{\mathbf{x}} = \begin{bmatrix} 9 \\ 8 \end{bmatrix} \text{ and } \Lambda_x = \sigma_x^{-2} \mathbf{I}_2,$$

where σ_x parameterizes the precision of $\bar{\mathbf{x}}$ in meters. The unknown position of the node is randomized as $\mathbf{x} \sim \mathcal{N}(\bar{\mathbf{x}}, \Lambda_x^{-1})$.

The resolution limits of SWINS, given by the HCRB (16), are shown in Fig. 9. When σ_x is 20 [cm] and the measurement noise level σ_k is 2 [ns], we note that the HCRB of ϕ_u reaches sub-nanosecond levels as the number of epochs k increases. The bound of T_m eventually collapses to that of T_u , whose accuracy is fundamentally limited by the errors of the timing device, cf. (7). In this scenario the online estimator achieves the HCRB for all parameters.

Fig. 9 illustrates also how the accuracy of the initial position estimate $\bar{\mathbf{x}}$, namely σ_x , limits the accuracy of ϕ_u . For 500 epochs, a position accuracy about ± 50 cm ($\sigma_x = 0.25$) results in sub-nanosecond resolution limit for ϕ_u . The bounds for T_m and T_u are left virtually unaffected by σ_x .

B. Master node with three transceivers

The unknown position of the node is fixed at $\mathbf{x} = [9 \ 8]^\top$. The resolution limits of SWINS, given by the CRB in (14), are shown in Fig. 10. For a noise level of $\sigma_k = 2$ [ns], the CRB of ϕ_u reaches sub-nanosecond levels already at 10 epochs. Similar to the previous scenario the online estimator attains the bounds, which now decrease steadily with the number of epochs.

Fig. 10 illustrates also how the measurement noise level limits the accuracy of ϕ_u . The estimation errors decrease as the unknown noise decreases $\sigma_k \rightarrow 0$. A small gap to the CRB for ϕ_u is visible when the noise level increases to 5 [ns].

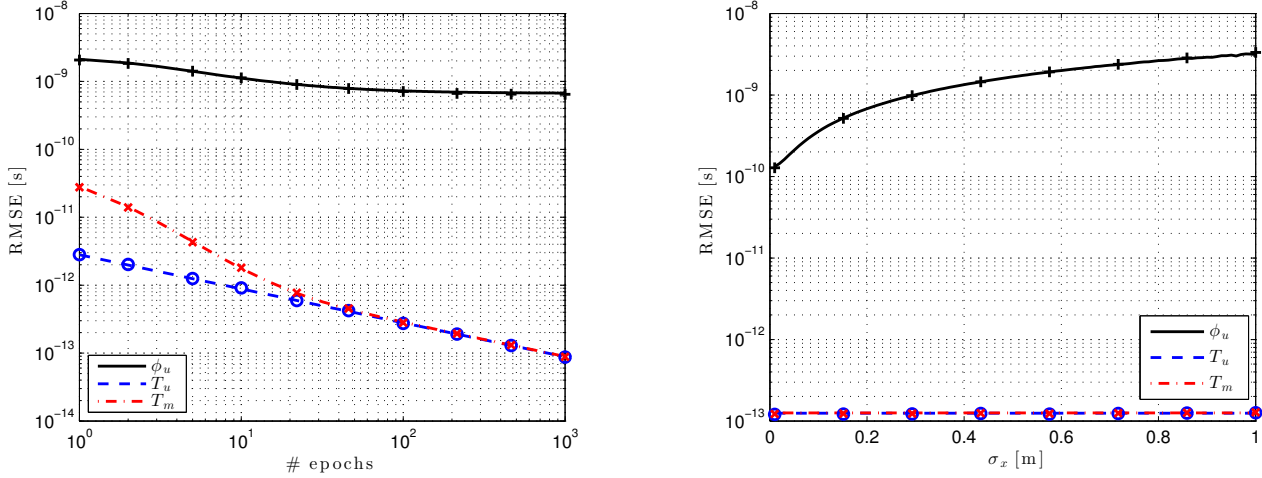


Fig. 9. Master without transceivers: System resolution limits (HCRB as lines) and estimator performance (crosses and circles) as a function of epochs (left) and precision of prior (right), respectively. The noise variance is σ_k is fixed to 2 [ns]. (Left) σ_x is 0.20 [m]. (Right) Number of epochs is 500.

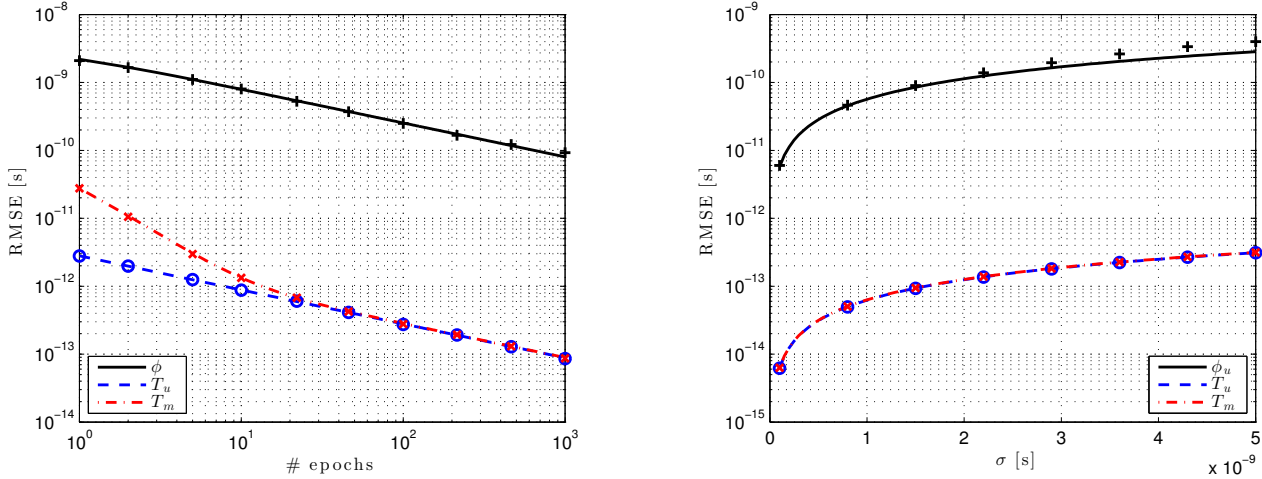


Fig. 10. Master with transceivers: System resolution limits (CRB as lines) and estimator performance (crosses and circles) as a function of epochs (left) and noise level (right), respectively. (Left) σ is 2 [ns]. (Right) Number of epochs is 500.

VI. CONCLUSION

We have designed a scalable system, denoted SWINS, in which an indefinite number of receiving wireless units can synchronize to a single master clock. The synchronization is performed at the level of discrete clock ticks and the mechanism can be implemented with passive receivers, thereby obviating the need for two-way communication and time-stamp exchanges.

By deriving Cramer-Rao bounds for the data model we can conclude that SWINS advances the limits wireless synchronization towards sub-nanoseconds levels based on state-of-the art hardware components. An online estimator based on the maximum likelihood approach was also developed that can operate with prior position information or, when such information is absent, with the proposed positioning infrastructure. The numerical experiments show that the estimator is statistically efficient.

In future work we will consider applications which can benefit from precise timing information and, furthermore, study the impact on performance of the geometric configuration of the transmitting nodes.

APPENDIX A DERIVATION OF GRADIENT

The gradient of V_1 is readily obtained as

$$\partial V_1 = \frac{2}{n} \mathbf{\Lambda}_x (\mathbf{x} - \bar{\mathbf{x}}). \quad (27)$$

Due to the logarithm $\ln V_0$, we can equivalently redefine V_0 as $V_0 = n\bar{\sigma}^2$. Then to obtain the gradient of $V_0(\mathbf{x})$ we first re-write the function as

$$V_0 = \boldsymbol{\rho}^\top \mathbf{W} \boldsymbol{\rho} - 2\mathbf{w}^\top \boldsymbol{\rho} + (\mathbf{y} - \boldsymbol{\mu})^\top \mathbf{Q}^{-1} \boldsymbol{\Pi}_H^\perp (\mathbf{y} - \boldsymbol{\mu}), \quad (28)$$

where

$$\mathbf{W} = c^{-2} \mathbf{G}^\top \mathbf{Q}^{-1} \mathbf{\Pi}_H^\perp \mathbf{G}$$

$$\mathbf{w} = c^{-1} \mathbf{G}^\top \mathbf{Q}^{-1} \mathbf{\Pi}_H^\perp (\mathbf{y} - \boldsymbol{\mu}).$$

Because (28) equals

$$V_0 = \sum_i \sum_j [\mathbf{W}]_{ij} \rho_i \rho_j - 2 \sum_i w_i \rho_i + K,$$

where K is a constant, the gradient can be expressed as

$$\partial V_0 = \sum_i \sum_j [\mathbf{W}]_{ij} (\gamma_i \rho_j + \rho_i \gamma_j) - 2 \sum_i w_i \gamma_i, \quad (29)$$

where

$$\gamma_i \triangleq \partial_x \rho_i = \partial_x (\|\mathbf{x} - \mathbf{x}_i\|^2)^{1/2} = \frac{\mathbf{x} - \mathbf{x}_i}{\|\mathbf{x} - \mathbf{x}_i\|}.$$

The gradients in (29) and (27) are used in (25).

REFERENCES

- [1] H. Meyr, M. Moeneclaey, and S. Fechtel, *Digital Communication Receivers: Synchronization, Channel Estimation, and Signal Processing*. John Wiley & Sons, Inc., 1997.
- [2] A. J. Viterbi, *CDMA: principles of spread spectrum communication*. Addison Wesley Longman Publishing Co., Inc., 1995.
- [3] R. Mudumbai, D. Brown, U. Madhow, and H. Poor, "Distributed transmit beamforming: challenges and recent progress," *Communications Magazine, IEEE*, vol. 47, no. 2, pp. 102–110, February 2009.
- [4] S. Lee, A. Gerstlauer, and R. Heath, "Distributed real-time implementation of interference alignment with analog feedback," *Vehicular Technology, IEEE Transactions on*, vol. 64, no. 8, pp. 3513–3525, Aug 2015.
- [5] P. Zetterberg and N. Moghadam, "An experimental investigation of SIMO, MIMO, interference-alignment (IA) and coordinated multi-point (CoMP)," in *Systems, Signals and Image Processing (IWSSIP), 2012 19th International Conference on*, April 2012, pp. 211–216.
- [6] O. El Ayach, S. Peters, and J. Heath, R.W., "The practical challenges of interference alignment," *Wireless Communications, IEEE*, vol. 20, no. 1, pp. 35–42, February 2013.
- [7] V. Chandrasekhar, J. Andrews, and A. Gatherer, "Femtocell networks: a survey," *Communications Magazine, IEEE*, vol. 46, no. 9, pp. 59–67, September 2008.
- [8] W.-Q. Wang, "GPS-based time phase synchronization processing for distributed SAR," *Aerospace and Electronic Systems, IEEE Transactions on*, vol. 45, no. 3, pp. 1040–1051, July 2009.
- [9] A. Catovic and Z. Sahinoglu, "The cramer-rao bounds of hybrid toa/rss and toa/rss location estimation schemes," *Communications Letters, IEEE*, vol. 8, no. 10, pp. 626–628, Oct 2004.
- [10] M. Pajic, S. Sundaram, G. J. Pappas, and R. Mangharam, "The wireless control network: A new approach for control over networks," *IEEE Trans. Automatic Control*, vol. 56, no. 10, pp. 2305–2318, 2011.
- [11] D. Mills, "Internet time synchronization: the network time protocol," *Communications, IEEE Transactions on*, vol. 39, no. 10, pp. 1482–1493, Oct 1991.
- [12] J. Han and D.-K. Jeong, "A practical implementation of IEEE 1588-2008 transparent clock for distributed measurement and control systems," *Instrumentation and Measurement, IEEE Transactions on*, vol. 59, no. 2, pp. 433–439, Feb 2010.
- [13] J.-L. Ferrant and S. Ruffini, "Evolution of the standards for packet network synchronization," *Communications Magazine, IEEE*, vol. 49, no. 2, pp. 132–138, February 2011.
- [14] J. Elson, L. Girod, and D. Estrin, "Fine-grained network time synchronization using reference broadcasts," *ACM SIGOPS Operating Systems Review*, vol. 36, no. SI, pp. 147–163, 2002.
- [15] S. Ganerwal, R. Kumar, and M. B. Srivastava, "Timing-sync protocol for sensor networks," in *Proceedings of the 1st International Conference on Embedded Networked Sensor Systems*, ser. SenSys '03. New York, NY, USA: ACM, 2003, pp. 138–149. [Online]. Available: <http://doi.acm.org/10.1145/958491.958508>
- [16] H. Dai and R. Han, "Tsync: a lightweight bidirectional time synchronization service for wireless sensor networks," *ACM SIGMOBILE Mobile Computing and Communications Review*, vol. 8, no. 1, pp. 125–139, 2004.
- [17] R. J. Anderson, "GPS synchronization for wireless communications stations," Sep. 22 2009, US Patent 7,593,738.
- [18] J. Elson and D. Estrin, "Time synchronization for wireless sensor networks," in *Parallel and Distributed Processing Symposium., IEEE Proceedings 15th International*, April 2001, pp. 1965–1970.
- [19] T. N. Osterdock, D. C. Westcott, and Q. D. Hua, "GPS synchronized frequency/time source," Aug. 8 1995, US Patent 5,440,313.
- [20] M. Segura, S. Niranjanayam, H. Hashemi, and A. Molisch, "Experimental demonstration of nanosecond-accuracy wireless network synchronization," in *Communications (ICC), 2015 IEEE International Conference on*, June 2015, pp. 6205–6210.
- [21] N. M. Freris, H. Kowshik, and P. R. Kumar, "Fundamentals of large sensor networks: Connectivity, capacity, clocks, and computation," *Proceedings of the IEEE*, vol. 98, no. 11, pp. 1828–1846, 2010.
- [22] B. Etzlinger, H. Wymeersch, and A. Springer, "Cooperative synchronization in wireless networks," *Signal Processing, IEEE Transactions on*, vol. 62, no. 11, pp. 2837–2849, 2014.
- [23] K.-l. Noh, E. Serpedin, and K. Qaraqe, "A new approach for time synchronization in wireless sensor networks: Pairwise broadcast synchronization," *Wireless Communications, IEEE Transactions on*, vol. 7, no. 9, pp. 3318–3322, 2008.
- [24] O. Jean and A. J. Weiss, "Passive localization and synchronization using arbitrary signals," *Signal Processing, IEEE Transactions on*, vol. 62, no. 8, pp. 2143–2150, 2014.
- [25] S. Dwivedi, A. De Angelis, and P. Handel, "Scheduled UWB pulse transmissions for cooperative localization," in *Ultra-Wideband (ICUWB), 2012 IEEE International Conference on*, Sept 2012, pp. 6–10.
- [26] S. Dwivedi, D. Zachariah, A. De Angelis, and P. Handel, "Cooperative decentralized localization using scheduled wireless transmissions," *Communications Letters, IEEE*, vol. 17, no. 6, pp. 1240–1243, June 2013.
- [27] D. Zachariah, A. De Angelis, S. Dwivedi, and P. Handel, "Self-localization of asynchronous wireless nodes with parameter uncertainties," *Signal Processing Letters, IEEE*, vol. 20, no. 6, pp. 551–554, June 2013.
- [28] D. Zachariah, A. D. Angelis, S. Dwivedi, and P. Händel, "Schedule-based sequential localization in asynchronous wireless networks," *EURASIP Journal on Advances in Signal Processing*, vol. 2014, no. 1, pp. 1–12, 2014. [Online]. Available: <http://dx.doi.org/10.1186/1687-6180-2014-16>
- [29] I. Skog and P. Händel, "Synchronization by two-way message exchanges: Cramer-rao bounds, approximate maximum likelihood, and offshore submarine positioning," *Signal Processing, IEEE Transactions on*, vol. 58, no. 4, pp. 2351–2362, 2010.
- [30] Y.-C. Wu, Q. Chaudhari, and E. Serpedin, "Clock synchronization of wireless sensor networks," *Signal Processing Magazine, IEEE*, vol. 28, no. 1, pp. 124–138, 2011.
- [31] J. Zhang, P. Orlik, Z. Sahinoglu, A. Molisch, and P. Kinney, "Uwb systems for wireless sensor networks," *Proceedings of the IEEE*, vol. 97, no. 2, pp. 313–331, Feb 2009.
- [32] C. Falsi, D. Dardari, L. Mucchi, and M. Z. Win, "Time of arrival estimation for uwb localizers in realistic environments," *EURASIP Journal on Advances in Signal Processing*, vol. 2006, no. 1, pp. 1–13, 2006.
- [33] S. Dwivedi, A. De Angelis, D. Zachariah, and P. Händel, "Joint ranging and clock parameter estimation by wireless round trip time measurements," *IEEE J. Selected Areas in Communications*, vol. 33, no. 11, pp. 2379–2390, 2015.
- [34] S. Kay, *Fundamentals of Statistical Signal Processing, Vol.1—Estimation theory*. Prentice Hall, 1993.
- [35] P. Stoica and R. L. Moses, *Spectral analysis of signals*. Pearson/Prentice Hall Upper Saddle River, NJ, 2005.
- [36] H. Van Trees, *Detection, Estimation, and Modulation Theory*, ser. Detection, Estimation, and Modulation Theory. Wiley, 2004, no. pt. 1. [Online]. Available: <https://books.google.se/books?id=Xzp7VkuFqXYC>
- [37] T. Kailath, A. H. Sayed, and B. Hassibi, *Linear Estimation*. Prentice-Hall, Inc., 2000.